RSC Advances

ROYAL SOCIETY OF CHEMISTRY

www.rsc.org/advances

Using a Functional C_{84} Monolayer to Improve the Mechanical Properties and Alter Substrate Deformation

W. S. Su[1], M. S. Ho[2,3], C. P. Huang[4], C. F. Chou[2], J. H. Tsai[1], and W. J. Lee[2,5*]

[1]National Center for High-Performance Computing, Hsinchhu 30076, Taiwan

[2]Department of Physics, National Chung Hsing University, Taichung 40227, Taiwan

[3]Institutes of Nanoscience, National Chung Hsing University, Taichung 40227, Taiwan

[4]Physics Division, Institute of Nuclear Energy Research, Taoyuan 325, Taiwan

[5]National Center for High-Performance Computing, Taichung 40763, Taiwan

Abstract

The nanoindentations of a silicon (111) substrate covered with a manipulated C_{84} monolayer are explored by molecular dynamics (MD) simulation calculations and further verified by experiment. Calculations show that pop-in events and stick-slip event are exhibited in the C_{84}/Si substrate during the loading process, where the pop-in events are caused by the severe deformation of the C_{84} molecule, while the stick-slip event takes place at the interface between tip and C_{84} molecule. The resulting deformed conformations and mechanical properties influenced by the diverse indentation mechanisms are also presented. Such a nanoindentation simulation model provides a powerful way to understand at an atomic level the interaction of the parts of an interface, and of the system as a whole. The experimental measurements from ultra-high vacuum atomic force microscopy (AFM) are compared with theoretical findings. Our investigations offer a possible replacement for semiconductor carbide.

*Corresponding author. E-mail: wjlee@nchc.narl.org.tw (W. J. Lee)

1. Introduction

In recent years, the various physical and chemical characteristics of silicon carbide (SiC), which bonds carbon and silicon, have been studied for prospective uses in the semiconductor industry[1]. Such SiC is a wide bandgap semiconductor with extreme properties including wear/corrosion resistivity, high breakdown field, high current density and high thermal conductivity, which make it a promising material for device applications that are integral to high-temperature, high-power circuit elements[2, 3, 4]. Further, SiC possesses abundant properties such as high strength, high hardness, high elastic modulus, superior chemical inertness, excellent thermal stability, which are crucial for mechanical, chemical, and aerospace applications.

A large area single SiC crystal synthesized using the Acheson process and Lely method approach[5, 6] is generated mainly in the temperature range of 1700 ℃ to 2700 ℃, with temperatures above 2500 ℃ necessary to obtain high purity single crystal SiC. Regulating pressure throughout the different stages is also a very important factor for Lely method manufacturing. Although a large area single SiC crystal can be easily synthesized, its crucial problem of a high density of defects in substrate materials has still not been solved. In addition, these defects (micropipes and dislocations) could propagate into device structures and cause device failure, resulting in a decay of the electric transport property. As a result, we have developed a synthetic version of SiC by embedding C_{84} fullerene molecules into a silicon substrate surface rather than by compaction of SiC films or nanocrystals[7, 8, 9].

In 1985, Kroto *et al*. found a 32-sided molecule formed of 60 carbon atoms (C_{60}), named a Buckminster fullerene or "Buckyball," whose diameter is 7.1Å [10]. Several fullerene molecules composed of spherical or spheroidal clusters of cage-like carbon molecules, such as C_{70}[11], C_{76}[12], C_{82}[12], and C_{84}[14], among others, have been either predicted or discovered. Among of them, 24 possible isomers of C_{84} have been reported, according to theoretical prediction[13, 14]. D2d(23) and D2(22) have been found to be the most stable and the second-most stable isomer. D2d(23) is 44-sided (32 hexagons and 14 pentagon sides) and has a symmetry-breaking dimension of 9 x7 Å, so as to result in large interaction forces between C_{84} molecules and a silicon substrate. In addition, these C_{84} molecules can be further embedded into a silicon substrate surface and gradually form a hexagonal closed-packed array on the silicon substrate due to the advantages of a self-assembly mechanism[15]. The measured properties of a synthetic C_{84} monolayer on the silicon substrate (C84/Si) are comparable to that of SiC. [16] For example, the bandgap of

C84/Si is 3.14eV, whereas that of SiC is 3.03~3.26eV. The breakdown electric field of C84/Si (for field emission application) is 4x106 V/cm, whereas that of SiC is 2.2~2.4x106 V/cm. Unlike SiC, C84/Si exhibits chemical inertness and a ferromagnetic property, which can enhance the stability of a system and extend the opportunity for advanced semiconductor applications. Therefore, this monolayer fullerene on Si thin film is proposed to scale down the size of current electronic device in a nano device, in contrast to the SiC substrate. In addition, the dramatic change in properties makes possible not only in the application of electronic device but also in that of optoelectronic[16], batteries[17], new generation photo-resists[18, 19], non-volatile memories[20], and cutting tool material.

Nanoindentation is widely used as a measurement technique for exploring the mechanical properties of surface layers of bulk materials and of thin films. Nanoindentation can elucidate the mechanical properties on a small scale, as the elastic modulus and stiffness can be observed, as well as allowing for measurement of the sample hardness, wear resistance and adhesion characteristics[21, 22]. In the indentation stiffness tests, a sharp indenter is forced into the surface of the material while measuring the force imposed and the corresponding displacement of the indenter. The mechanical characteristics can therefore be measured directly by the force and displacement without observing the surface; accordingly, the nanoindentation method is useful in capturing the mechanical features of surfaces and films on a small scale[23, 24].

In this article, molecular dynamics (MD) simulation calculations are employed to model nanoindentation in the investigation of a monoloayer of $C_{84}(D_{2d})23$ fullerene molecules on a Si(111) surface. It is found that pop-in events are displayed in the C_{84}/Si substrate during the loading process and are illustrated. The simulations reveal enhanced mechanical properties as well as diminished structural deformation of the substrate. The results of nanoindentation derived from simulation modelling are qualitatively examined with ultra-high vacuum atomic force microscopy (AFM) measurements[15]. The findings show that a silicon surface fabricated with an embedded monolayer of C_{84} may serve as a successor to silicon carbide materials.

2. Methodology

In this work, the mechanical properties of a C_{84}/Si substrate were determined by nanoindentation and compared with those of a pure Si substrate. Simulation models of the C_{84}/Si specimen of the equilibrium structure of the C_{84} monolayer embedded into the Si

surface were prepared by the following four-step procedure. (1) A Si (111) 7x7 surface was annealed from 1550 K to room temperature at a cooling rate of 3 K/ps. (2) The 49 C_{84} molecules were arranged in a honeycomb structure. The C_{84} molecules were confined in two repulsive walls and an equilibrium process was performed at 700K for 200ps. The system temperature was then annealed to room temperature. (3) The C_{84} monolayer was placed on the annealed Si substrate. A repulsive wall was placed upon the C_{84} monolayer and used to press the C_{84} monolayer into the Si surface. The system was then equilibrated at 1100K for 40ps and annealed to room temperature. (4) Finally, the silicon probe with a diameter of 5nm was positioned above the C_{84} monolayer at a distance of 5.0 Å, and allowed to move downward toward the specimen at a specified velocity. The final equilibrium model is illustrated in Fig. 1, which shows the indentation model of a C_{84} monolayer embedded into the Si (111) substrate. For the Si specimen model, we used the annealed Si substrate model as the indentation specimen, as was prepared in step 1 of the C_{84}/Si model procedure.

Molecular dynamics (MD) code, LAMMPS[25], developed by Sandia National Laboratories, was employed to study the indentations of the C_{84} monolayer embedded into the Si (111) substrate. As shown in Fig. 1, the silicon substrate with thickness of 8 nm has a top Newtonian atom layer, a thermal control layer, and a bottom fixed layer. The Newtonian atom layer, thermal control layer, and fixed layer are 0.7, 2, and 5.3 nm thick, respectively. The C_{84} monolayers were also modeled as a Newtonian atom. The indentation probe, composed of 1734 silicon atoms, was assumed to be a rigid body. Consequently, the silicon atoms in the probe are in rigid body motion during the simulation. The simulation boxes were rhomboid in shape with periodic boundary conditions in the x- and the y-directions. The dimensions of simulation boxes were L_x=108.1 Å, L_y=93.6 Å and L_Z=140 Å. The Nosè-Hoover method[26] is adopted to ensure the system remains at the desired temperature, and the velocity-verlet algorithmwas employed to predict the trajectories of the atoms. A time step of 0.2 fs was set for the time integration. In the present study, the AIREBO potential[27] is employed to simulate the inter-atomic forces between the carbon atoms in the C_{84}, while the Tersoff potential[28] is utilized to model the Si-Si and Si-C interactions.

For the experiment section, a Si substrate was pre-annealed at 800 ^{o}C for 30 minutes. A fullerene overlayer was deposited on top of this substrate in an ultra-high vacuum (UHV) held at a pressure of less than $5x10^{-8}$ Pa at 650^{o}C via a K-cell (Vacweld, Miniature K-cell). The resulting flat, self-assembled single layer of fullerene C_{84} molecules on the Si(111) surface was then investigated using a variable temperature scanning probe

microscope (JSPM-4500VT), as can be seen in our previous work[15, 16]. For UHV-STM imaging, we employed a sample bias voltage and tunneling current of -2V and 0.1nA, respectively. A UHV atomic force microscope (AFM) (JSPM-4500VT) was employed to evaluate the nanomechanical properties on the surface using Si probes with radius of ~5-20 nm and spring constants of ~43 N/m and ~ 26 N/m at a resonant frequency of ~300 kHz.

The Young's modulus and surface stiffness extracted from the force-distance curve of indentation is based on Oliver and Pharr's method[22]. An elastic recovery is expected after the load is released. A linear relation can be derived between the Young's modulus and the unloading stiffness of the probe. The stiffness (i.e., the slope of the initial portion) of the unloading curve is defined as

$$S = \frac{dP}{dh} = \beta \frac{2}{\sqrt{\pi}} \sqrt{A} E_r$$

where P, h, A, and E_r are the indentation load, elastic displacement of probe, projected area of the indentation, and reduced modulus. β (=1 for circular indenter) is the shape modification factor. The Young's modulus can be written as

$$\frac{1}{E_r} = \frac{(1 - v^2)}{E} + \frac{(1 - v_i^2)}{E_i}$$

where E and *v* are the Young's modulus and Poisson's ratio for the specimen and E_i and v_i are the same parameters for the indenter. The hardness, representing the material's ability to resist local deformation, is defined as $H = P_{max}/A$, where P_{max} is the maximum indentation force. To measure the stress of the C_{84} and the silicon substrate under indentation, atomic level stress[29] is employed, which includes kinetic and potential effects.

The indentation process includes four sub-processes—loading, holding, unloading, and retraction. During the indentation process, the probe moves downward to the specimen at a constant speed of 10 m/s until the specific loading depth. Such a velocity is suitable to observe[30] and describe the plastic deformation behavior and material properties under nanoindentation because our results can be recognized as approximately quasi-static in nature[31]. Consequently, the results obtained from simulation are suitable for comparison with those from experiment. After that, the probe is held static for 100 ps to allow for relaxation of the atoms. Finally, the probe is extracted.

3. Results and Discussion

The C_{84} monolayer coverage effect on the mechanical properties of Si substrate has been investigated by indentation tests. Figure 2 (a) and (b) plots the loading-displacement curves of C_{84}/Si and Si specimens related to different indentation depths. The curves indicate that the silicon indenter has a slight adhesive force on the surface of the specimen before the indenter contacts the specimen. Figure 3 (a) depicts the enlarged force-distance curve of the C_{84}/Si and the snapshots of the motion behavior of the C_{84} molecules under indentation. The C_{84} molecules exhibit the jump-to-contact phenomenon when the indenter approaches the C_{84} monolayer as shown in label (ii) of Fig. 3 (b). As the indenter continually drops and contacts the C_{84} molecules, the configuration of the C_{84} molecules gradually sink, as demonstrated in label (ii) of Fig. 3(b). Carrying back to Fig. 2, the evolution of force-distance curves in the elastic-deformation regime is found to approximately follow a Hertzian behavior for the Si specimens, where the indentation force is proportional to the indentation depth. Only a slight fluctuation is found on the curves. Compared to the curves of C_{84}/Si specimen, the loading curve increases with significant fluctuations, as two pop-in events are observed at depths of –4.5~ –7 and –16~ –19Å and the several force drops are found at depth of about –9.5, –13.5, -17, –22.8, and–27 Å. Both pop-in events can be associated with the deformation of the C_{84} molecules. The force drops correspond to the stick-slip motion of the C_{84} molecules/indenter interface and the plastic yielding event and nucleation of silicon atoms below the C_{84} layers. To verify that the pop-in events and stick-slip motion are attributed to the molecular behaviour of C_{84} molecules, Fig. 4 presents the individual contact stress-distance curves of the Si substrate and the C_{84} molecule of the C_{84}/Si specimen.

Note that the stress of Si substrate increases with slight fluctuation as the indentation depth increases. The result can attributed to the relaxation and local nucleation of the silicon atoms, which will be discussed in the following paragraph. However, it should be stressed that the stress of C_{84} increases with significant variation, which can be divided into linear, pop-in, and transition states, behaving in different deformation mechanisms. In linear state ranged in depth between 0 and -5 Å, it shows a linear relationship between the pressure and the indentation depth, where the compressed C_{84} molecules undergo an elastic deformation process as can be seen in Fig. 5(a) to (b). The two pop-in states (ranged in depth between–4.5~ –7 and –16~ –19Å) drawn in Fig. 4, as depicted in Fig. 2, cause an obvious severe deformation of the cluster shape when a loading force is exerted upon them, which, therefore, releases the exerting force. The corresponding snapshots of

before and after pop-in states for the C_{84} layers are illustrated in Fig. 5(b)-(c) and (d)-(e).The shape of the C_{84} molecules gradually transform from a cage structure with smooth surface to a bowl-like structure with zigzag surface. When it drop into the transition state ranged in depth between -7and -16 Å, the C_{84} molecules surrounding the bowl-like C_{84} molecules exhibits the partial deformation and stick-slip motion at the C_{84} molecules/indenter interface. Consequently, the fluctuation of the contact pressure represents a periodic cycle of alternating motion. A similar phenomenon has been found in the friction of the graphene by friction force microscopy experiment.[32]

To clearly understand the effect of the C_{84} layer on the structural deformation of the silicon substrate under indentation, the distributions of the von Mises strain (ε_{vM}) of all atoms are calculated and drawn in Fig. 6 (a) and (b), where the C_{84}/Si and silicon specimen are at the maximum indentation depth of –10 Å, and have undergone the first pop-in event for C_{84}/Si. The blue color ($\varepsilon_{vM} < 0.14$) represents the atoms in the elastic deform region, while colors ranging from green to red indicate the defect atoms in the plastic deform region. As for the C_{84}/Si specimen, note that the C_{84} monolayer sinks into the silicon substrate. A pile-up event is not observed during the indentation, even at an indentation depth of –30 Å, which implies that the stiffness of C_{84} is more than that of the silicon surface. Moreover, through the von Mises strain analysis, we found that the C_{84}/Si specimen has a wider elastic deformation region than the Si specimen. The phase transformation regions were identified and displayed in terms of coordination numbers (CN), shown in Fig. 6 (c) and (d), so that a portion of diamond cubic silicon with CN=4 transforms to CN=5 in the deformation region. Comparing the C_{84}/Si and Si specimens, we found that the CN=5 Si atoms of the C_{84}/Si specimen have a lower density and a wider range of distribution than in the Si specimen. This can be attributed to the hollow structure of the C_{84} fullerene molecule that plays a role of a cushion and disperses the compression stress on the silicon substrate as a result of inducing a wider region of elastic deformation. In the following unloading process, pop-out events are observed around –8 and –3Å, as shown in Fig. 2(a). A portion of CN=5 phase are transformed to the original diamond structure phase for both C_{84}/Si and Si specimen, which is illustrated in the inset of Fig. 2(b). For the case of C_{84}/Si, adhesion associated with the interaction between the probe and C_{84} clusters resulted in damage to the surface structure following retraction of the probe.

Figure 7 shows the snapshots of the indentation process with maximum indentation depth of –10 Å. Some of the deformed C_{84} structures will be restored to their cage structure in the unloading process, as shown in Fig. 7(c). It should be noted that previous

study[33] has reported that a free fullerene has been found to exhibit elastic behavior even if the different radii of fullerenes in the direction of compression are reduced to 1/2 that of free fullerenes. In the retraction process, the C_{84} molecules were uprooted by the probe, as indicated in Fig. 7(d) and (e). This result was later confirmed by AFM indentation as demonstrated in Fig. 8 with the plot of the snapshots of the C_{84}/Si surface before (Fig. 8(a)) and after (Fig. 8(b)) AFM indentation. In the AFM images, the two circles in white indicate reference positions which verify the same region in the two images, while the three crosses are the indentation locations. It is obvious that a portion of C_{84} fullerenes disappears from the Si substrate after the indentation, as can be seen in Fig. 8(b).

The maximum indentation force, unloading stiffness, hardness, reduced modulus, and Young's modulus are computed for both C_{84}/silicon and silicon specimens, and listed in Table I. Note that the Young's modulus of the C_{84}/Si specimens is not presented here because there is no simply determined method to compute the corresponding Poisson ratio for a nanostructure such as this, whose properties at nanoscale level may not be as predictable as those observed at larger scales. For the Si specimen with different indentation depths, the hardness and Young's modulus of ≈17~30 GPa and ≈177~252 GPa are close to those obtained from experiment (hardness of 21.2GPa for hc<1nm, hardness of 21~18.5GPa for 1nm<hc<5nm[34], and Young's modulus of 185GPa for silicon (111)[35]) as well as those from theoretical research (Young's modulus of 188.7GPa[36]). The maximum indentation force, unloading stiffness, reduced modulus, and Young's modulus all increase with increasing indentation depth. However, for the C_{84}/Si, the reduced modulus gradually decreases at indentation depth <–4.5 Å, but begins to increase again at indentation depth <–10 Å. These findings imply that the deformation of the C_{84} molecules or the pop-in events affects the magnitude of the reduced modulus. Furthermore, comparing the reduced modulus between the C_{84}/Si and Si specimens, we found that the coverage of C_{84} molecules can effectively increase the specimen's reduced modulus when the loading depth >–10 Å.

The loading stiffness with the depth of indentation was characterized using AFM and MD simulation force curves. In the AFM experiment, the probe with the larger spring constant resulted in surface indentations that were more pronounced. Surface elasticity played a key role when the probe first contacted the surface; however, the cantilever dominated the mechanical response as the probe notched more deeply into the surface. Thus, probes with a larger spring constant were able to present more information with regard to surface stiffness for indentation of a given depth. Figure 9 shows the loading stiffness of MD simulation and AFM experiment as a function of loading depth for C_{84}/Si.

The stiffness trend from MD simulation is the same as that in AFM measurements. In addition, the slope of stiffness-distance curve at a depth >–5 Å for both simulation and experiment is higher than that at a depth <–5 Å. These results imply that the coverage provided by a C_{84} monolayer effectively increase the surface stiffness. In addition, it is observed that the stiffness increases linearly at depth >–5 Å, whereas it increases with fluctuations at depths <–5 Å for both experiment and simulation. The fluctuations phenomena can be attributed to the influence of the pop-in events at depths of –4.5 ~–7 Å and –16Å ~–19Å as mentioned above, leading to the two-stage deformation of C_{84} molecules.

4. Conclusions

The mechanisms of a C_{84} monolayer on a silicon substrate under indentation have been investigated by molecular dynamics simulation and AFM experiment. The simulation results showed that the C_{84} molecules exhibit a jump-to-contact phenomenon when the indenter approaches the C_{84} monolayer. The coverage of C_{84} molecules increases the mechanical properties of the Si substrate, and also plays the role of a damper or cushion to disperses the compression stress on the substrate, which, therefore, induces the pop-in events and stick-slip motion in the compression process. The pop-in events, which lower the reduced modulus and loading stiffness, are observed due to the two-stage deformation of the C_{84} molecules. The stick-slip motion causes the significant force drops in the indentation curve. The phenomena found in the simulation results were further verified by AFM nanoindentation experiments qualitatively.

5. Acknowledgments

The authors would like to thank the Ministry of Science and Technology of Taiwan, for financially supporting this research under Contract Nos. MOST-102-2923-E-492-001-MY3 (W. J. Lee), NSC-101-2112-M-492-001-MY3 (W. S. Su) and NSC-102-2112-M-005-003-MY3 (M. S. Ho). Support from the National Centers for Theoretical Sciences (South) and High-performance Computing of Taiwan in providing huge computing resources to facilitate this research are also gratefully acknowledged.

6. References:

1. Davis, R. F. Epitaxial growth and doping of and device development in monocrystalline β-SiC semiconductor thin films. *Thin Solid Films* **1989,** *181*, 1-15

2. Morkoc, H.; Strite, S.; Gao, G. B.; Lin, M. E.; Sverdlov, B.; Burns, M. Large-band-gap SiC, III-V nitride, and II-VI ZnSe-based semiconductor device technologies. *J. Appl. Phys.* **1994,** *76*, 1363-1398.

3. Casady, J. B.; Johnson, R. W. Status of silicon carbide (SiC) as a wide-bandgap semiconductor for high-temperature applications: a review. *Solid-State Electronics* **1996,** *39* (10), 1409–1422.

4. Hornberger, J.; Lostetter, A. B.; Olejniczak, K. J.; McNutt, T.; Lal, S. M.; Mantooth, A. Silicon-carbide (SiC) semiconductor power electronics for extreme high-temperature environments. *Aerospace conference, 2004. Proceedings. 4*, 2538-2555.

5. Hofmann, D.; Schmitt, E.; Bickermann, M.; Kölbl, M.; Wellmann, P. J.; Winnacker, A. Analysis on defect generation during the SiC bulk growth process. *Materials Science and Engineering: B* **1999,** *61*, 48-53.

6. Ohtani, N.; Fujimoto, T.; Aigo, T.; Katsuno, M.; Tsuge, H.; Yashiro, H. Large high-quality silicon carbide single crystal substrate. *Nippon Steel Technical Report* **2001,** *84*, 36-41.

7. Wu, X. L.; Siu, G. G.; Stokes, M. J.; Fan, D. L.; Gu, Y.; Bao, X. M. Blue-emitting β-SiC fabricated by annealing C60 coupled on porous silicon. *Appl. Phys. Lett.* **2000,** *77*, 1292-1294.

8. Deng, S. S.; Wu, X. L.; Li, J.; Tan, C.; Yang, X.; Gu, Y.; Bao, X. M. Optical emission from annealed coupled-C60 porous Si systems. *J. Phys.: Cond Matter* **2002,** *14*, L739-L744.

9. Yan, F.; Bao, X. M.; Wu, X. W.; Chen, H. L. Photoluminescence spectra of C60 molecules embedded in porous Si. *Appl. Phys. Lett.* **1995,** *67*, 3471-3473

10. Kroto, H. W.; Heath, J. R.; O'Brien, S. C.; Curl, R. F.; Smalley, R. E. C60:Buckminsterfullerene. *Nature* **1985,** *318*, 162-163.

11. Buseck, P. R.; Tsipursky, S. J.; Hettich, R. Fullerenes from the Geological Environment. *Science* **1992,** *257* (5067), 215-217

12. Kawada, H.; Fujii, Y.; Nakao, H.; Murakami, Y.; Watanuki, T.; Suematsu, H.; Kikuchi, K.; Achiba, Y.; Ikemoto, I. Structural aspects of C82 and C76 crystals studied by x-ray diffraction. *Phys. Rev. B* **1995,** *51*, 8723-8730.

13. Fowler, W.; Manolopoulos, D. E. *An Atlas of Fullerenes*; Clarendon Press: Oxford 1995.

14. Akasaka, T.; Nagase, S. *Endofullerenes: A New Family of Carbon Clusters*; Kluwer Academic Press: Dordrecht, 2002. p p. 99. 2.

15. Huang, C. P.; Su, C. C.; Su, W. S.; Hsu, C. F.; Ho, M. S. Nanomeasurements of electronic and mechanical properties of fullerene embedded Si(111) surfaces. *Appl. Phys. Lett.* **2010,** *97*, 061908

16. Huang, C. P.; Su, W. S.; Su, C. C.; Ho, M. S. Characteristics of Si(111) surface with embedded C84 molecules. *RSC Advances* **2013,** *3*, 9234-9239.

17. Arie, A. A.; Lee, J. K. Fullerene C60 coated silicon nanowires as anode materials for lithium secondary batteries. *J Nanosci Nanotechnology* **2012** *12* (4), 3547-3551.

18. Gibbons, F. P.; Robinson, A. P. G.; Diegoli, S.; Manickam, M.; Preece, J. A.; Palmer, R. E. Fullerene Resist Materials for the 32nm Node and Beyond. *Adv. Funct. Mater.* **2008,** *18* 1977.

19. Manyam, J.; Manickam, M.; Preece, J. A.; Palmer, R. E.; Robinson, A. P. G. Plasma etching of high-resolution features in a fullerene molecular resist , . *Proc. SPIE* **2011,** *7972*.

20. Beckmeier, D.; Baumgärtner, H. Metal-oxide-semiconductor diodes containing C60 fullerenes for non-volatile memory applications. *Journal of Applied Physics* **2013,** *113*, 044520

21. Oliver, W. C.; Pharr, G. M. An improved technique for determining hardness and elastic modulus using load and displacement sensing indentation experiments. *J. Mater. Res.* **1992,** *7*, 1564-1583.

22. Pharr, G. M.; Oliver, W. C.; Brotzen, F. R. On the generality of the relationship among contact stiffness, contact area and elastic-modulus during indentation. *J. Mater. Res.* **1992,** *7*, 613.

23. Bhushan, B.; Koinkar, V. N. Nanoindentation hardness measurements using atomic force microscopy. *Appl. Phys. Lett.* **1994,** *64* (13), 1653

24. Saha, R.; Nix, W. D. Effects of the substrate on the determination of thin film mechanical properties by nanoindentation. *Acta Materialia* **2002,** *50*, 23–38.

25. S. J. Plimpton. Fast Parallel Algorithms for Short-Range Molecular Dynamics. *J. Comp. Phys.* **1995,** *117*, 1-19 URL: http://lammps.sandia.gov.

26. Rapaport, D. C. *The Art of Molecular Dynamics Simulations*; Cambridge University Press: Cambridge, 1997.

27. Stuart, S. J.; Tutein, A. B.; Harrison, J. A. A reactive potential for hydrocarbons with intermolecular interactions. *Journal of Chemical Physics* **2000,** *112* (14), 6472.

28. Tersoff, J. New empirical model for the structural properties of silicon. *Phys. Rev. Lett.* **1986,** *56*, 632.

29. Chandra, N.; Namilae, S.; Shet, C. Local elastic properties of carbon nanotubes in the presence of Stone-Wales defects. *Phys. Rev. B* **2004,** *69* (9), 094101.

30. Schulz, M. J.; Kelkar, A. D.; Sundaresan, M. J. Nanoengineering of Structural, Functional and Smart Materials. *Taylor & Francis* **2005**, 736.

31. Ju, S. P.; Wang, C. T.; Chien, C. H.; Huang, J. C.; Jian, S. R. The Nanoindentation Responses of Nickel Surfaces with Different Crystal Orientations. *Molecular Simulation* **2007,** *33* (11), 905-917.

32. Yoon, H. M.; Jung, Y.; Jun, S. C.; Kondaraju, S.; Lee, J. S. Molecular dynamics simulations of nanoscale and sub-nanoscale friction behavior between graphene and a silicon tip: analysis of tip apex motion. *Nanoscale* **2015,** *7*, 6295-6303.

33. Zhang, Z. X.; Pan, Z. Y.; Wang, Y. X.; Li, Z. J.; Wei, Q. Simulations of the Nanomechanical Properties of Compressed Small Fullerenes. *Mod. Phys. Lett. B* **2003,** *17*, 877.

34. Garcia-Manyes, S.; Güell, A. G.; Gorostiza, P.; Sanz, F. Nanomechanics of Silicon Surfaces with Atomic Force Microscopy: An Insight to the First Sates of Plastic De- formation. *Journal of Chemical Physcs* **2005,** *123*, 114711.

35. Wortman, J. J.; Evans, R. A. Young's Modulus, Shear Modulus, and Poisson's Ratio in Silicon and Germanium. *Journal of Applied Physics* **1965,** *36*, 153

36. Choi, I. S.; Gan, Y.; Kaufmann, D.; Kraft, O.; Schwaiger, R. Measurement of Young's modulus of anisotropic materials using microcompression testing. *Journal of Materials Research* **2012,** *27* (21), 2752

Table Caption

Table 1：Mechanical properties of C84/Si and Si(111) specimens by nanoindentation. P_{max}, S, HD, E_r, and E indicate the maximum indentation force, unloading stiffness, hardness, reduced modulus, and Young's modulus, respectively.

Table 1

	Depth(Å)	Pmax(nN)	S (N/m)	HD(GPa)	E_r(GPa)	E(GPa)
C84/Si	–2.5	44.0	63.8	11.8	27.1	—
	–4.5	73.8	86.6	11.6	28.2	—
	–7.0	165.2	99.8	17.5	26.7	—
	–10.0	297.0	93.8	23.6	21.7	—
	–20.0	502.3	124.8	25.8	23.2	—
	–25.0	657.4	137.0	31.9	25.4	—
	–30.0	761.1	153.5	39.9	28.4	—
Si	–10.7	224.9	85.7	17.1	19.4	180.9
	–20.7	437.2	121.1	22.9	22.8	212.8
	–25.7	509.0	127.4	25.9	23.6	236.2
	–30.7	570.1	145.8	29.0	27.0	252.1

Figure Caption

FIG. 1: (a) Simulation model of C_{84} monolayer on Si substrate. (b) Enlarged view of C_{84} molecules embedded into the Si surface.

FIG. 2: Force-distance curves for different indentation depths for (a) C_{84}/Si (left panel) and (b) Si (111) specimens (right panel).

FIG. 3: (a) Enlarged force-distance curves for C84/Si (left panel). (b) The corresponding snapshots of the C84 molecules at different indentation distances, where the probe is not shown (right panel).

FIG. 4: Contact stress-distance curves of the C_{84} molecule and Si substrate of the C_{84}/Si specimen.

FIG. 5: Cross-sectional view of the indentation depth at (a)0 Å, (b)–4.5 Å, (c)–7 Å, (d)–16 Å, and (e)–19 Å. (b) to (c) and (d) to (e) depict the pop-in process, whereas (c) to (d) represent the transition process. The C_{84} molecular structure is sliced to illustrate the deformation for clearly display. The arrows in red and blue indicate the C84 molecules with plastic (bowl-like structure) and elastic deformation, respectively.

FIG. 6: The von-Mises strain distribution of (a) C_{84}/Si and (b) Si(111) specimens at indentation depth of –10 Å, where values lower than 0.08 and higher than 0.25 are not shown. Panels (c) and (d) are the corresponding coordination number distribution of C_{84}/Si and Si(111) specimens.

FIG. 7: Indentation process of C_{84}/Si for the case of maximum depth of–10 Å. Panels (a)-(e) show the snapshots at corresponding distances, labelled a-e in Fig. 2.

FIG. 8: AFM images of C_{84}/Si surface (a) before and (b) after the indentation at 25x25nm resolution. The two circles in white indicate reference positions that verifies the two images are the same region, while the three crosses are the locations of the AFM indentation.

FIG. 9: Loading stiffness determined by MD simulations and AFM experiments as a function of distance for (a) C_{84}/Si and (b) Si(111) specimens. The arrows indicate the sink points that represent the weakening of stiffness.

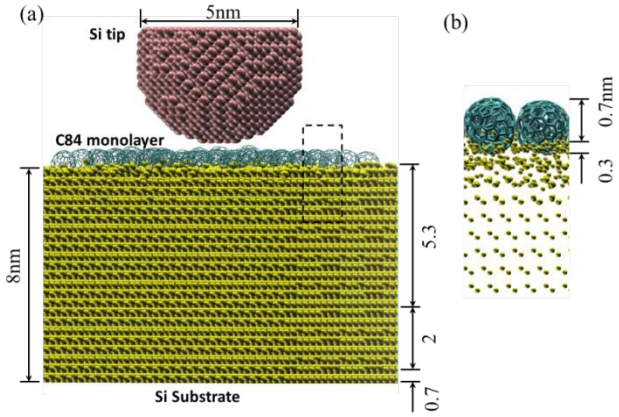

FIG. 1

(a)

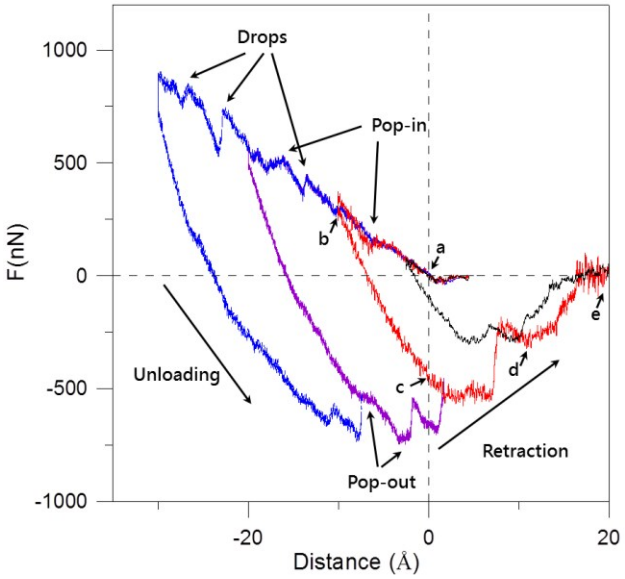

(b)

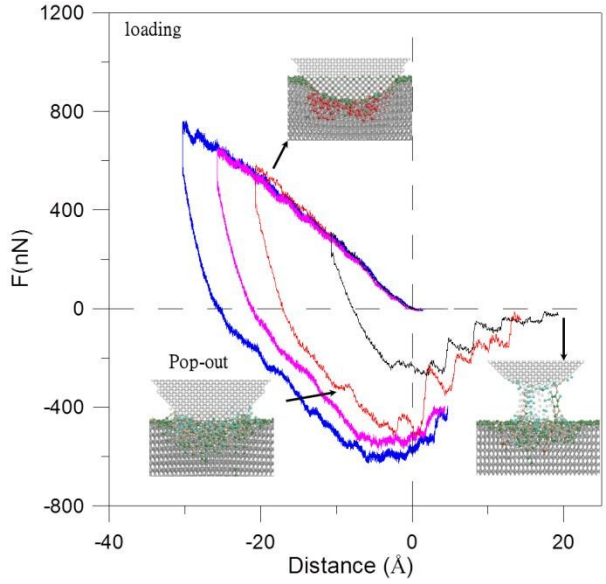

FIG. 2

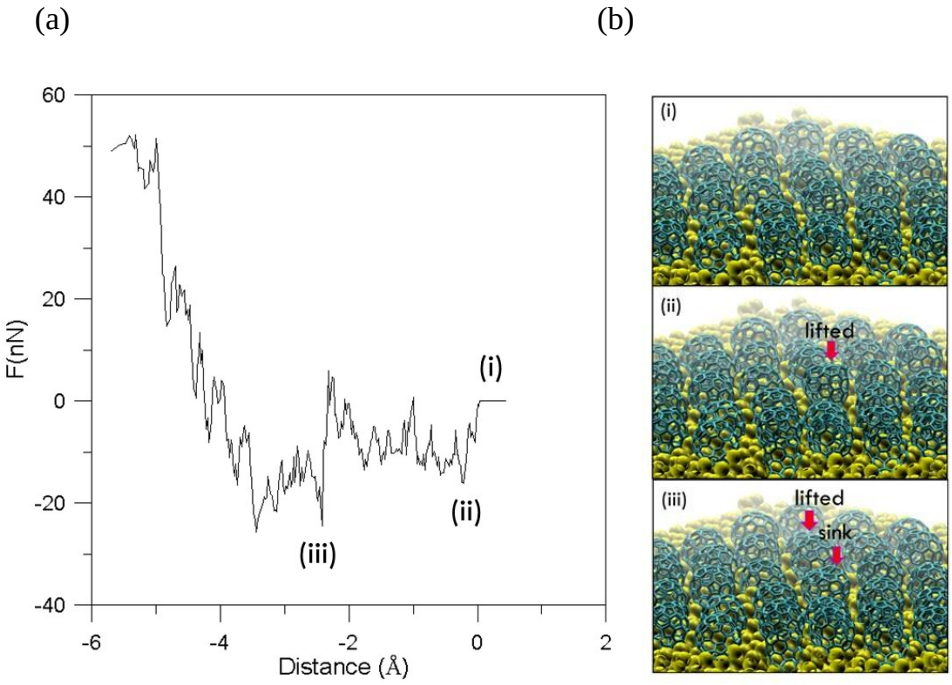

FIG. 3

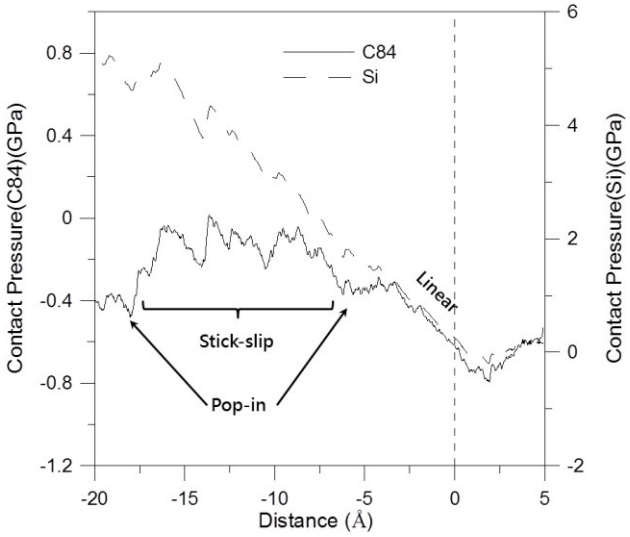

FIG. 4

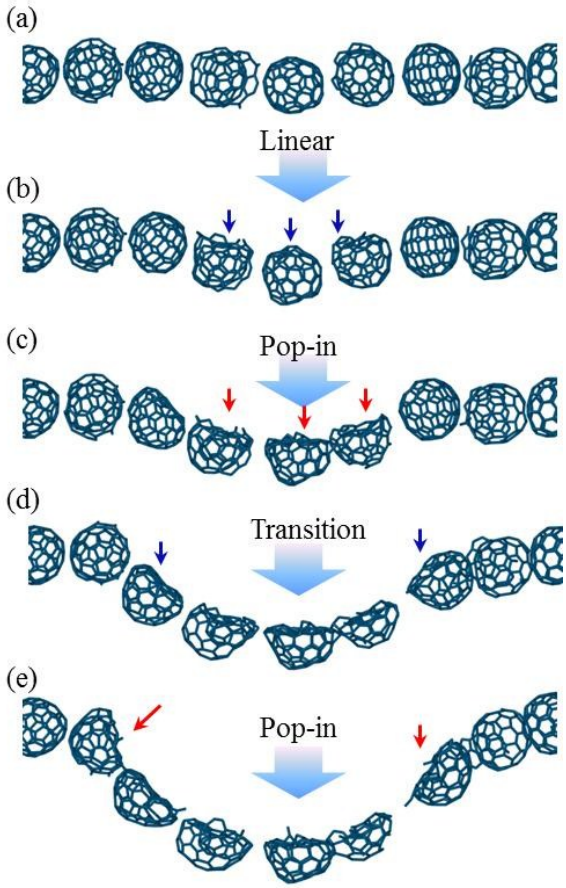

FIG. 5

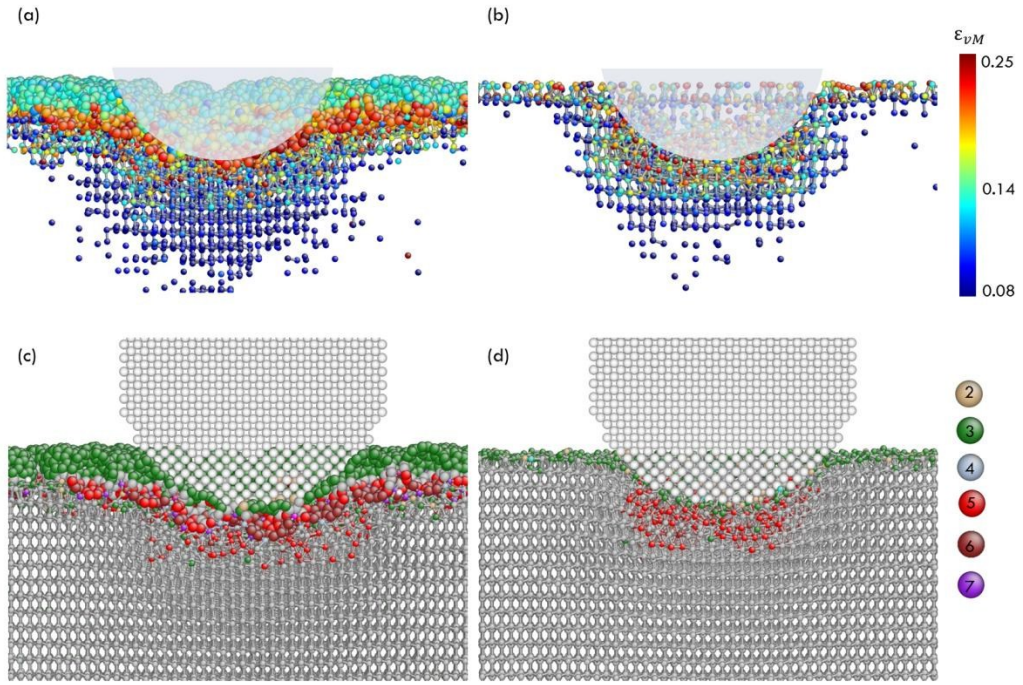

FIG. 6

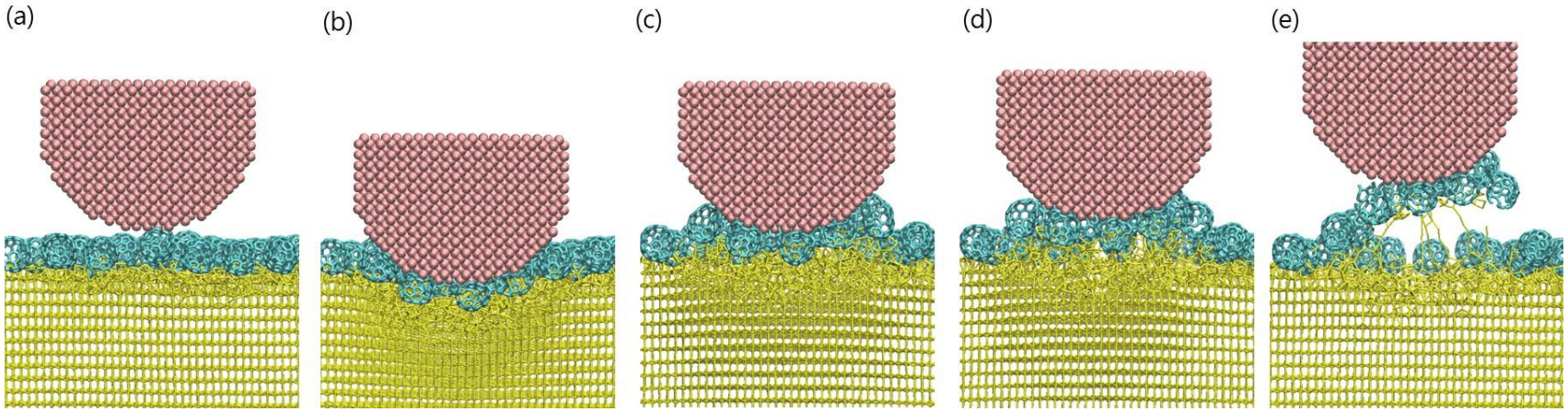

FIG. 7

(a) (b)

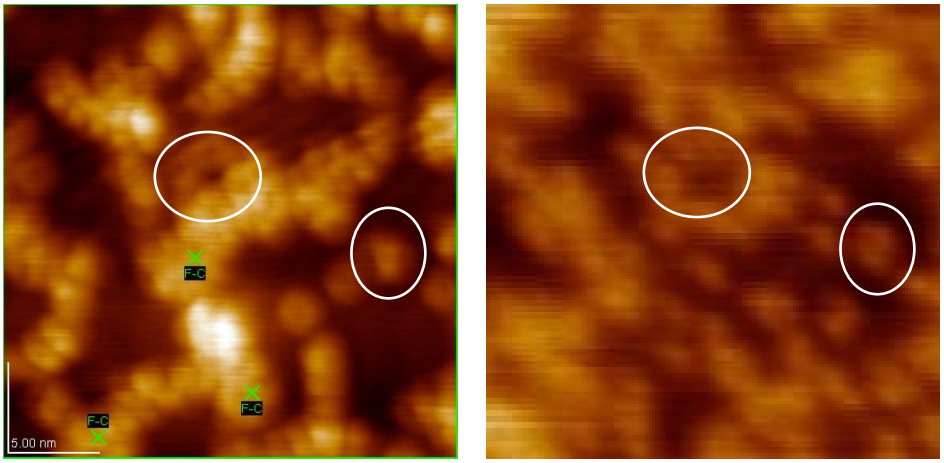

FIG. 8

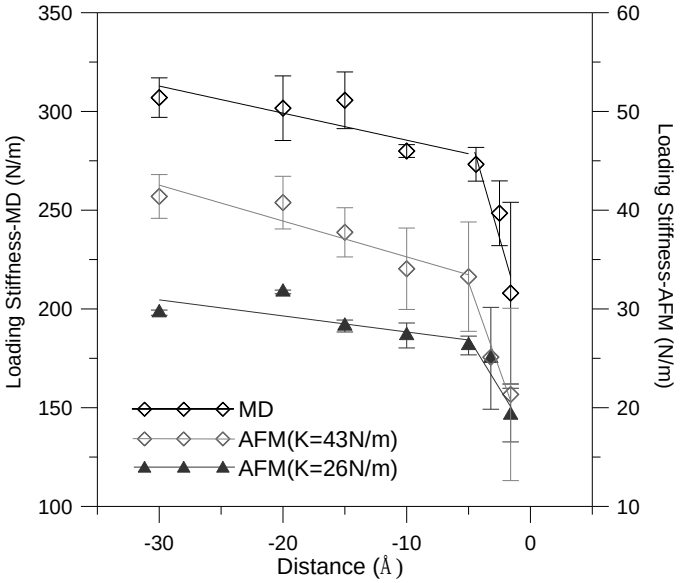

FIG. 9